The dc to ac Josephson transition in a dc atom SQUID

H. M. Cataldo

IFIBA-CONICET

and

Departamento de Física,

FCEN-UBA Pabellón 1,

Ciudad Universitaria,

1428 Buenos Aires, Argentina

Abstract

We analyze the effect of the barrier motion on the Bose-Hubbard Hamiltonian of a ring-shaped Bose-Einstein condensate interrupted by a pair of Josephson junctions, a configuration which is the cold atom analog of the well-known dc superconducting quantum interference device (SQUID). Such an effect is also shown to modify the Heisenberg equation of motion of the boson field operator in the two-mode approximation, where a hysteretic contribution that could affect the dynamics for accelerated or overlapping barriers is identified. By studying the energy landscape as a function of order and control parameters, we determine the diagram with the location of the dc and ac Josephson regimes, along with the critical points that are shown to depend on the junctions position. We analyze the dc to ac Josephson transition for adiabatic barrier trajectories that lead to a final uniform velocity, or which perform symmetric velocity paths. We show that such symmetric trajectories may induce, when reaching the critical point, highly hysteretic oscillating return paths within the dc regime, similar to the underdamped hysteresis loops arising from the action of a resistive flow in the ac regime. We also consider nonequilibrium initial conditions resulting from a finite phase difference on either side of the junctions, along with the critical features of such a parameter. An excellent agreement between the Gross-Pitaevskii simulations and the two-mode results is found in all cases.

I. INTRODUCTION

A direct current superconducting quantum interference device (dc-SQUID) basically consists of a ring of superconducting wire interrupted by two non-superconducting barriers (Josephson junctions). Wire leads connected to each side of the device act as a splitter and a recombiner, as a steady bias current flowing from the splitter enters the ring and gives rise to the quantum interference of currents emerging from each Josephson junction (JJ) at reaching the recombiner [1]. A magnetic field threading the ring causes a phase shift between both currents, an effect which may be utilized to implement a magnetic flux detector. As a result, dc-SQUIDs constitute today the most sensitive detectors for magnetic flux available [1]. On the other hand, in a superfluid, the role of the magnetic field is played by rotation, and superfluid helium dc-SQUIDs acting as rotation sensors have been experimentally implemented [2]. More recently, a cold atom analog of the dc-SQUID was created on a toroidal Bose-Einstein condensate (BEC), which works as follows [3–5]. By slowly moving a pair of JJs circumferentially toward each other, there is an induced atom flow through the junctions that keeps the density and the chemical potential unchanged at both sides of the barriers. This is in close analogy to the superconducting dc Josephson effect, where a direct current may flow across a JJ without a driving potential difference [6–8]. However, if the speed of the junctions exceeds certain value such that the induced atom flow through them reaches the Josephson critical current, the condensate dynamics makes a transition to the ac Josephson regime, where there is an oscillating current through the JJs but no net current across them. Therefore, under these conditions the moving barriers simply push the atoms, resulting in compression of atoms in one sector of the condensate and expansion in the other. Such a difference on densities yields different values of the chemical potential at both sectors. Again, this dynamics is analog to the ac Josephson effect in superconductors, where a constant voltage across a JJ produces an alternating current [6–8]. The experimental demonstration of the dc and ac Josephson effects in a dilute BEC was first proposed in Ref. [9] and later effectively carried out by utilizing a single JJ in relative motion with respect to the harmonic trap [10]. The authors also discussed the experimental feasibility of an atom dc-SQUID, in particular its eventual application as a rotation sensor based on the dependence of the critical current on the condensate rotation rate [10]. On the other hand, a similar dc-SQUID-type experimental setup with a pair of counterrotating weak links instead

of the tunnel junctions was implemented in Ref. [11] to study the microscopic origin of the resistive flow appearing when the superfluid current reaches the critical value. Previously, an important variant of these experiments had been carried out for a single rotating weak link [12], which is essentially analogous to a rf-SQUID. Such a configuration, which also has the potential to be utilized as a sensitive rotation sensor, was demonstrated to possess quantized hysteresis, in the first observation of such a phenomenon in a superfluid BEC [13].

In this work, we analyze the dc to ac Josephson transition in an atom dc-SQUID similar to that of the experimental setup in Ref. [3]. Our theoretical study makes use of Gross-Pitaevskii (GP) simulations and a two-mode (TM) model, where only the ground state and the first-excited stationary state of an asymmetric double-well toroidal condensate are taken into account to build the dynamics [14]. Note that such a model is not expected to describe accurately a far from equilibrium configuration like that occurring in the ac Josephson regime, nor an eventual transition from ac to dc. The TM model applied to an asymmetric double-well toroidal condensate was discussed in Ref. [14], where important effective interaction effects were incorporated in the model parameters [15, 16]. On the other hand, the time dependence of the potential barriers (moving JJs), required to recreate the Josephson dc and ac regimes, should give rise to a time-dependent boson field operator (in the Schrödinger representation) that would yield extra terms in the Heisenberg and derived equations of motion (GP, TM). This suggests that the simplest starting point to study this issue could be to build a Bose-Hubbard (BH) Hamiltonian in a TM approximation. In fact, we derive extra terms due to the barrier motion in such a Hamiltonian, as well as a hysteretic additional contribution to the Heisenberg equation of motion of the boson field operator in the TM approximation. The BH Hamiltonian in the limit of a macroscopic occupation of states yields a condensate energy depending on an order parameter, represented by the phase difference and the particle imbalance, and a control parameter, represented by the position and velocity of the JJs. The study of such an energy landscape allows to find the location of the regions where the dc and ac Josephson effects are expected to occur, along with the corresponding critical points.

We have considered two kinds of barrier motion. In the first one, an adiabatic initial acceleration leads to a final uniform velocity that ultimately yields the dc to ac transition. The second kind shares the same initial acceleration protocol up to reaching a maximum velocity, from where there is a symmetric decceleration leading to a final symmetric rest

position of the barriers. Barrier trajectories of this kind allow to observe the hysteretic effects that take place when the condensate gets quite close to the dc-ac transition. Such effects are found to be similar to those occurring for faster barrier trajectories able to drive the condensate from the dc to the ac regime and, in the subsequent stage of barrier decceleration, bring it back to the dc regime via the action of a resistive flow. Similar hysteretic processes are common in superconducting JJs [17, 18] and have been studied within the frame of the resistively and capacitively shunted junction (RCSJ) model [19]. In our case, taking note of the close analogy between such a model and a TM model with damping [20], we have analyzed the hysteresis loops that should take place as a result of the action of ac resistive flows.

This paper is organized as follows. In the next section, we specify the technical details of the physical system considered in this study, along with the corresponding GP simulations. Section III treats the BH model and the TM equations of motion, starting with a review of the case with barriers at rest in Sec. III A, and next by extending the treatment to the case of moving barriers in Sec. III B. The energy landscape, which allows to locate the regions belonging to the dc and ac regimes, is analyzed in Sec. III B 1, while the dc-ac transition and related hysteresis effects for several adiabatic barrier trajectories are dealt with in Sec. III B 2. Finally, a comparison between the GP simulations and the TM model results is performed in Sec. III B 3, while some concluding remarks are gathered in Sec. IV.

II. THE SYSTEM AND GP SIMULATIONS

We describe in what follows the system utilized in our simulations and model applications. All the trapping parameters and condensate details have been chosen to reproduce the experimental setting of Ref. [3]. The trapping potential can be written as the sum of a part that depends only on x and y and a part that is harmonic in the tightly bound direction z:

$$V_{\rm trap}(x,y,z) = V(x,y) + \lambda^2 z^2/2 \tag{1}$$

being

$$V(x,y) = V_{\rm T}(r) + V_{\rm B}\,(x,y). \tag{2}$$

The above potential consists of a superposition of a toroidal term $V_{\rm T}(r)$ ($r^2 = x^2 + y^2$) and the radial barrier term $V_{\rm B}\,(x,y)$. The toroidal potential was modeled through the following

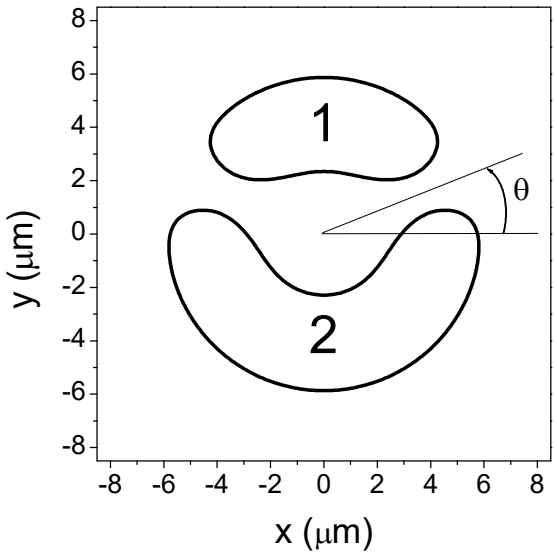

FIG. 1. Particle density isocontours for the ground state of N=3000. The barrier positions correspond to $\theta = \pi/8$.

Laguerre-Gauss optical potential [21]

$$V_{\rm T}(r) = V_0 \left[1 - \left(\frac{r^2}{r_0^2}\right) \exp\left(1 - \frac{r^2}{r_0^2}\right)\right], \tag{3}$$

where V_0 corresponds to the depth of the potential and r_0 the radial position of its minimum.

The barriers were modeled as

$$V_{\rm B}(x,y) = V_b \sum_{k=1}^{2} \exp\left\{-\frac{[y\cos\theta_k - x\sin\theta_k]^2}{\lambda_b^2}\right\} \Theta[y\sin\theta_k + x\cos\theta_k], \tag{4}$$

where Θ denotes the Heaviside function with $\theta_1 = \theta$ and $\theta_2 = \pi - \theta$. The parameter θ (see Fig. 1) may depend on time according to the barriers movement, and the following system parameters were utilized [3]: $V_0/k_B = 70$ nK, $r_0 = 4$ μm, $V_b/k_B = 41.07$ nK, $\lambda_b = 1\,\mu$m and N=3000 atoms of ^{87}Rb. We have used in our GP simulations scaled units referenced to the unit of length $L_0 = 1$ μm, which yields energy and time units given by $E_0/k_B = \hbar^2/(k_B m L_0^2) = 5.5298$ nK and $T_0 = \hbar/E_0$ =1.3813 ms, respectively, where m denotes the mass of a condensate atom. We have assumed a high value of λ in Eq. (1), $(\lambda L_0)^2 = 64\,E_0$, yielding a quasi-bidimensional condensate and allowing a simplified numerical treatment [22]. So, the adimensionalized condensate order parameter is written as the product of a Gaussian wave function along the z coordinate, $\sqrt{\frac{\lambda^{1/2}}{\pi^{1/2}}}\, e^{-\frac{\lambda z^2}{2}}$, and a two-dimensional (2D) wave function $\psi(x,y,t)$ normalized to one, for which the corresponding GP equation in

scaled units reads

$$i\frac{\partial\psi}{\partial t} = -\frac{1}{2}\left(\frac{\partial^2\psi}{\partial x^2} + \frac{\partial^2\psi}{\partial y^2}\right) + V(x,y)\,\psi + gN\,|\psi|^2\psi, \tag{5}$$

where the effective $2D$ coupling constant $g = \sqrt{\frac{\lambda}{2\pi}}g_{3D}$ is written in terms of the coupling constant between the atoms $g_{3D} = \frac{4\pi\hbar^2 a/m}{E_0 L_0^3} = 4\pi a/L_0$, with $a = 98.98\,a_0$ the s-wave scattering length of ^{87}Rb and a_0 the Bohr radius. Such a GP equation was solved using the split-step Crank-Nicolson method [23] on a 2D spatial grid of 171×171 points.

III. BH MODEL AND TM EQUATIONS OF MOTION

A. Barriers at rest

We begin by reviewing in this section the TM equations of motion for the toroidal asymmetric double-well condensate with barriers at rest derived in Ref. [14]. However, in contrast to the previous treatment, we will start here from a BH model in order to facilitate a generalization to the case of moving barriers in the next section.

The following BH Hamiltonian arises as usual from the many-body second-quantized Hamiltonian written in terms of the TM approximation of the boson field operator $\hat{\Psi}(x,y) = \psi_1(x,y)\hat{a}_1 + \psi_2(x,y)\hat{a}_2$ [24], where $\psi_k(x,y)$ denotes the real wave function of a boson localized in the k-well with a corresponding annihilation operator denoted by $\hat{a}_k$,

$$\begin{aligned}\hat{H}_{BH} = {} & \varepsilon_1\hat{a}_1^\dagger\hat{a}_1 + \varepsilon_2\hat{a}_2^\dagger\hat{a}_2 + K(\hat{a}_1^\dagger\hat{a}_2 + \hat{a}_2^\dagger\hat{a}_1) + \frac{U_1}{2}\hat{a}_1^\dagger\hat{a}_1^\dagger\hat{a}_1\hat{a}_1 + \frac{U_2}{2}\hat{a}_2^\dagger\hat{a}_2^\dagger\hat{a}_2\hat{a}_2 \\ & + F_{12}(\hat{a}_1^\dagger\hat{a}_1^\dagger\hat{a}_1\hat{a}_2 + \hat{a}_1^\dagger\hat{a}_2^\dagger\hat{a}_1\hat{a}_1) + F_{21}(\hat{a}_2^\dagger\hat{a}_2^\dagger\hat{a}_1\hat{a}_2 + \hat{a}_1^\dagger\hat{a}_2^\dagger\hat{a}_2\hat{a}_2) \\ & + \frac{S}{2}(\hat{a}_1^\dagger\hat{a}_1^\dagger\hat{a}_2\hat{a}_2 + \hat{a}_2^\dagger\hat{a}_2^\dagger\hat{a}_1\hat{a}_1 + 4\hat{a}_1^\dagger\hat{a}_2^\dagger\hat{a}_1\hat{a}_2),\end{aligned} \tag{6}$$

where

$$\varepsilon_k = \int d^2r\ \psi_k(x,y)\left[-\frac{\hbar^2}{2m}\nabla^2 + V(x,y)\right]\psi_k(x,y), \tag{7}$$

$$K = -\int d^2r\ \psi_1(x,y)\left[-\frac{\hbar^2}{2m}\nabla^2 + V(x,y)\right]\psi_2(x,y), \tag{8}$$

$$U_k = g\int d^2r\ \psi_k^4(x,y), \tag{9}$$

$$F_{jk} = -g\int d^2r\ \psi_j^3(x,y)\psi_k(x,y), \tag{10}$$

$$S = g \int d^2r \; \psi_1^2(x,y)\, \psi_2^2(x,y). \tag{11}$$

Here it is important to remark that such localized states, characterized by the wave functions $\psi_k(x,y)$ and the corresponding operators $\hat{a}_k$ and $\hat{a}_k^\dagger$, may actually depend on the number of particles at each well. Particularly, as a most significant effect of the repulsive interparticle interaction, there is a broadening of the wave functions ψ_k with increased occupation numbers [24, 25]. However, since the occupation number variations for our time evolutions in the dc Josephson regime, including the transition to the ac regime, actually keep small enough, we will disregard, in principle, such a dependence in the Hamiltonian (6). Nevertheless, in the following we shall see that the above interaction effects may be taken into account at the level of the TM equations of motion, in order to get a substantial improvement in the agreement with the GP simulation results.

The Hamiltonian (6) rules the condensate dynamics according to the Heisenberg equations,

$$\frac{d\hat{a}_k}{dt} = \frac{i}{\hbar}[\hat{H}_{BH}, \hat{a}_k], \tag{12}$$

and assuming a macroscopic occupation of states, one may replace the annihilation operators by complex c-numbers,

$$\hat{a}_k \to \sqrt{N_k}\, \exp(i\phi_k), \tag{13}$$

where ϕ_k and N_k represent the phase and particle number in the k-well, respectively. By performing such a replacement in (12) one may obtain the following equations of motion of the TM model, where the time evolution of the condensate is described through the particle imbalance $Z = (N_2 - N_1)/N$ and the phase difference between both wells $\phi = \phi_1 - \phi_2$ (see Fig. 1),

$$\hbar\dot{Z} = -\frac{\Delta E}{(1-Z_0^2)^{3/2}}\sqrt{1-Z^2}\,(1 - 2Z_0^2 + Z_0 Z)\sin\phi + NS\,(1-Z^2)\sin(2\phi) \tag{14}$$

$$\begin{aligned}\hbar\dot{\phi} = {} & (Z - Z_0)\left[N(U_1+U_2)/2 + \frac{\Delta E}{(1-Z_0^2)^{3/2}}\frac{(1+2Z_0 Z)}{\sqrt{1-Z^2}}\cos\phi - 2NS\right] \\ & + NS[Z_0 - Z\cos(2\phi)]\,,\end{aligned} \tag{15}$$

where $\Delta E = N(F_{21} - F_{12})(1-Z_0^2)^{3/2}/Z_0$ denotes the energy-per-particle splitting between both stationary solutions of the above equations of motion, namely the ground state with $\phi = 0$ and the first-excited state with $\phi = \pm\pi$, both states having the same imbalance

$Z = Z_0$, whose value depends on the barrier angle θ. Such states, which correspond to the stationary solutions of the GP equation (5) yielding the lowest condensate energies, can be expressed as linear combinations of the localized states,

$$\psi_{\pm} = \pm\sqrt{\frac{1-Z_0}{2}}\psi_1 + \sqrt{\frac{1+Z_0}{2}}\psi_2, \tag{16}$$

where ψ_+ (ψ_-) denotes the wave function of the ground (first-excited) single-particle state. However, such wave functions are not mutually orthogonal, except for a symmetric configuration ($\theta = 0$ in Fig. 1) [14]. In fact, for a whole population N in the ground (first-excited) single-particle state, there would be NZ_0^2 atoms in the first-excited (ground) single-particle state.

The hopping contributions proportional to the energy gap ΔE and the parameter S in (15), turn out to be quite negligible with respect to the term proportional to the average on-site interaction energy $(U_1 + U_2)/2$, so we may adopt such an approximation in Eq. (15). In addition, we have seen in Ref. [14] that the agreement between the TM time evolution results and the GP simulations turns out to be substantially improved by replacing such an average on-site interaction energy by the following expression,

$$U + BZ \tag{17}$$

with

$$\begin{aligned} U &= \frac{1}{2}[(1-\alpha_1)U_1 + (1-\alpha_2)U_2)] \\ B &= \frac{1}{2}(\alpha_1 U_1 - \alpha_2 U_2)\,, \end{aligned} \tag{18}$$

where the parameters α_j arise from the deformation that suffer the condensate densities at both wells due to the departure of the particle imbalance Z from the stationary value Z_0 during the time evolution. In fact, denoting by $\rho_j^{(\Delta N_j)}$ the probability density of the localized state at site j with $N_j^0 + \Delta N_j$ particles, where N_j^0 denotes the population of the j-well corresponding to the imbalance Z_0, the parameter α_j may be obtained from the following modified on-site interaction energy parameter [14–16]

$$\begin{aligned} U_j^{(\Delta N_j)} &= g\int d^2r\ \rho_j^{(0)}(x,y)\,\rho_j^{(\Delta N_j)}(x,y) \\ &\simeq (1 - 2\alpha_j\frac{\Delta N_j}{N})U_j, \end{aligned} \tag{19}$$

where $\rho_j^{(0)} = \psi_j^2$ and the second line corresponds to the first-order approximation on $\Delta N_j/N$, being $2\Delta N_2/N = -2\Delta N_1/N = Z - Z_0$. To extract, in practice, the parameter α_j, one should numerically evaluate the above integral with a probability density $\rho_j^{(\Delta N_j)}(x, y)$ obtained from the stationary states of a condensate with $N_j^0 + \Delta N_j$ particles on the site j and a total number of particles that differs from N [14–16]. The idea behind such calculations is that a nonequilibrium state should be well aproximated by localized on-site states corresponding to the instantaneous populations at each well. Thus, the replacement in Eq. (15) of the average on-site interaction energy $(U_1 + U_2)/2$ by the imbalance-dependent parameter $U + BZ$, serves to quantitatively taking into account the above density variations. It is important to remark that the contributions arising from the parameters α_j in (18) turn out to be far from negligible, despite of being originated at the first-order approximation (19). In fact, such effective interaction corrections were found to substantially improve the agreement with the time-dependent GP simulation results [14]. Finally, we may rewrite the equation of motion (15) as,

$$\begin{aligned} \hbar\dot{\phi} &= (Z - Z_0)N(U + BZ) \\ &= \mu_2 - \mu_1, \end{aligned} \tag{20}$$

where μ_j denotes the chemical potential of the condensate at the site j. The above equivalence between the time derivative of the phase difference at both sides of a Josephson junction and the corresponding chemical potential difference has been shown to possess a wide range of validity [2, 10], and it is analogous to the voltage-phase relation of the Josephson effect in superconductors [6–8].

The condensate energy in the TM approximation may be obtained from the BH Hamiltonian (6) under the replacement (13), yielding

$$\begin{aligned} E_{TM} = {} & N\frac{(\varepsilon_1 + \varepsilon_2)}{2} + N^2\frac{(U_1 + U_2)}{4}\left(\frac{1 + Z^2}{2} - Z_0 Z\right) \\ & - \frac{\sqrt{1 - Z^2}}{2(1 - Z_0^2)^{3/2}} N\Delta E(1 - 2Z_0^2 + ZZ_0)\cos\phi \\ & + \frac{N^2 S}{2}\left[(1 - Z^2)\left(1 + \frac{1}{2}\cos 2\phi\right) + 3Z_0 Z\right]. \end{aligned} \tag{21}$$

However, it will be more convenient to measure the energy relative to that of the ground-state ($Z = Z_0$, $\phi = 0$), which yields

$$\Delta E_{TM} \equiv E_{TM} - E_{TM}^{GS} = N^2\frac{(U_1 + U_2)}{8}(Z - Z_0)^2$$

$$+\frac{N}{2}\Delta E\left[1-\frac{\sqrt{1-Z^2}}{(1-Z_0^2)^{3/2}}(1-2Z_0^2+ZZ_0)\cos\phi\right]$$
$$+\frac{N^2S}{2}\left\{(1-Z^2)\left(1+\frac{1}{2}\cos 2\phi\right)+\frac{3}{2}[2Z_0Z-(1+Z_0^2)]\right\}, \quad (22)$$

where it is worthwhile noticing that the first-excited single-particle state ($Z = Z_0$, $\phi = \pm\pi$) yields the correct energy gap $\Delta E_{TM} = N\Delta E$ in (22). Note also that the equations of motion (14)-(15) can be written in the Hamiltonian form

$$\hbar\dot{N}_2 = -\frac{\partial\mathcal{H}}{\partial\phi}\ ;\ \hbar\dot{\phi} = \frac{\partial\mathcal{H}}{\partial N_2}, \quad (23)$$

being $\mathcal{H} = \Delta E_{TM}$ the Hamiltonian and (N_2,ϕ) the canonically conjugate variables. Here it is instructive to approximate the expression (22) for $Z \simeq Z_0$, along with neglecting the term proportional to the second-order hopping parameter S. Thus, taking into account Eq. (15) without the tunneling contributions, we obtain the following Hamiltonian for a "phase particle" of coordinate ϕ

$$\mathcal{H} \simeq \frac{\hbar^2\dot{\phi}^2}{2(U_1+U_2)} + \frac{N\Delta E}{2}(1-\cos\phi), \quad (24)$$

where the first and second term should be interpreted as the kinetic and potential energy, respectively. Note that the minimum and maximum of the potential energy at $\phi = 0$ and $\phi = \pm\pi$, respectively, correspond to the above stationary states, as expected. A similar expression is found for the Hamiltonian of a superconducting Josephson junction in the low damping limit, which may be quantized through a straightforward procedure to investigate the quantum behavior of the phase difference [26, 27]. However, such quantum effects turn out to be quite negligible in our case, since the frequency ω_p of the low amplitude (plasma) oscillations around the potential minimum, yielding the level spacing $\hbar\omega_p = \sqrt{N\Delta E(U_1+U_2)/2}$, turns out to be much smaller than the depth of the potential well $N\Delta E$, a result which agrees with the classical picture represented by the Hamilton equations (23).

B. Moving barriers

If the barriers are set in motion, there are two effects that could modify the Heisenberg equation for the boson field operator $\hat{\Psi}$. The first effect stems from the additional contribution to the many-body Hamiltonian arising from the induced particle flux across the

moving barriers. A second effect should arise from the time dependence of the boson field operator in the Schrödinger representation due to the barrier motion. Let us first discuss the additional contribution to the energy. In fact, as barriers are displaced, the change in the particle number of each localized state causes a local energy change at a rate given by the corresponding chemical potential $\mu_j = \partial E_j/\partial N_j$. So, taking into account such contributions, the additional energy may be written,

$$\int_{N_1^{\rm ref}}^{N_1} \mu_1 \, dN_1' + \int_{N_2^{\rm ref}}^{N_2} \mu_2 \, dN_2' = \int_{N_2^{\rm ref}}^{N_2} (\mu_2 - \mu_1) \, dN_2',$$

where the values $N_j^{\rm ref}$ denote reference (initial) particle numbers. Note that have dropped the reference energies and have taken into account the constraint $N_1' + N_2' = N$ in the last equality. To proceed with the calculation, we may change variables in the last integral to the time domain and use (20) to obtain

$$\hbar \int_0^t \frac{d\phi}{dt'} \, I^0(t') dt',$$

where $I^0 \equiv \dot{N}_2^0 = (N/2)(\partial Z_0/\partial\theta)\,\dot{\theta}$ will be called the bias current, as it is kinematically dependent of the barrier motion, to distinguish from the actual particle current $I \equiv \dot{N}_2$. Next, we integrate the above result by parts in order to split it into an 'instantaneous' contribution,

$$\hbar I^0(t)\phi(t), \tag{25}$$

where we have dropped its initial value, and a hysteretic contribution,

$$-\hbar \int_0^t \dot{I}^0(t')\phi(t') dt', \tag{26}$$

which depends on the previous history of the system. Note that both contributions will be proportional to the time derivatives of the stationary imbalance $Z_0(\theta(t))$,

$$2\frac{I^0}{N} = \dot{Z}_0 = \frac{\partial Z_0}{\partial\theta}\,\dot{\theta}, \tag{27}$$

$$2\frac{\dot{I}^0}{N} = \ddot{Z}_0 = \frac{\partial^2 Z_0}{\partial\theta^2}\,\dot{\theta}^2 + \frac{\partial Z_0}{\partial\theta}\,\ddot{\theta}. \tag{28}$$

We depict in Fig. 2 such an imbalance as a function of the barrier angle θ, along with its first two derivatives. There we may observe that Z_0 presents a rather linear behavior, yielding a constant value for the first derivative and a negligible value for the second, except for barrier angles approaching 0.4π, where the barriers begin to overlap each other. Particularly, the

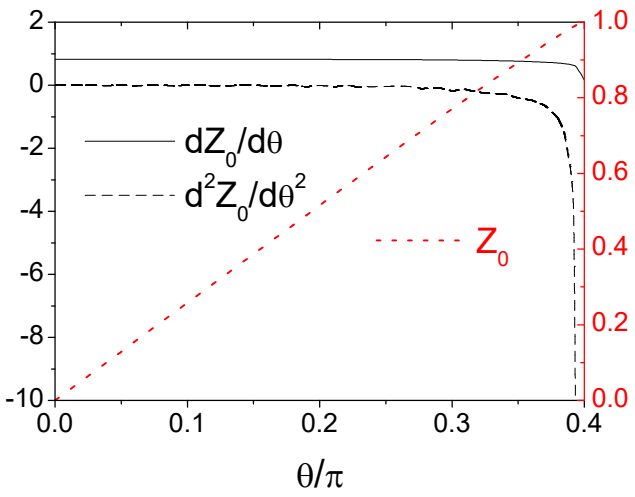

FIG. 2. The stationary imbalance Z_0 and its first two derivatives versus the barrier angle θ. The right scale corresponds to Z_0, while the left scale corresponds to its derivatives.

second derivative becomes clearly nonnegligible for such configurations. For instance, in the simplest situation of a barrier motion with a constant velocity, there would be an initial jump in velocity from the previous configuration of barriers at rest, which would yield a Dirac delta acceleration $\ddot{\theta} \sim \delta(t)$ in (28) and in the integrand of the expression (26). However, this contribution to the energy should be irrelevant, since it could be treated as a constant term. On the other hand, the first term of (28) could become nonnegligible for barrier angles approaching 0.4π, and this could eventually activate the hysteretic contribution (26) to the condensate energy.

The additional energy (25) has previously been considered in the context of an analogy with the RCSJ model, widely applied for superconducting Josephson junctions [6–10, 26–28]. However, its corresponding counterpart in the quantum many-body Hamiltonian, along with an eventual effect on the equations of motion, e.g., on the time-dependent GP equation, seem to be so far undiscussed. Here it is important to recall that experimental results on similar configurations of ring-shaped condensates with moving barriers, have shown a good agreement with the corresponding simulation results arising from the GP equation without any correction, apart from the time dependence of the trapping potential due to the moving barriers. Such experiments were conducted for different kinds of barrier motion, namely for adiabatic accelerations up to the final constant velocity [3], as well as for a sudden set into motion of the barriers at a constant speed [11].

Now, turning back to the theoretical arena, we should seek for an additional contribution to the Hamiltonian (6), which in the limit (13) of a macroscopic occupation, would yield the expression (25). A complete solution of this problem should be closely related to the long-standing and quite delicate issue of obtaining an acceptable quantum description of the phase by means of a phase operator [29]. Rather than pursuing such an ambitious goal, we will content ourselves with restricting our analysis to a limit of high populated localized states. In fact, let us consider the following operator,

$$\frac{i}{2}\left[\ln(\hat{a}_1^\dagger \hat{a}_2) - \ln(\hat{a}_2^\dagger \hat{a}_1)\right], \tag{29}$$

which would yield in the limit (13) just the phase difference ϕ. However, in defining the above expression one should take into account that the existence of the logarithm of a given operator must require that it should be invertible [30]. In particular, the creation and annihilation operators only partially fulfill such a requirement, since they turn out to be, similarly to the Susskind-Glogower phase operators [31], one-sided unitary, namely [32]

$$\hat{a}_k \hat{a}_k^{-1} = \hat{a}_k^{\dagger -1} \hat{a}_k^\dagger = \mathbf{I} \tag{30}$$

$$\hat{a}_k^{-1} \hat{a}_k = \hat{a}_k^\dagger \hat{a}_k^{\dagger -1} = \mathbf{I} - |0\rangle\langle 0|, \tag{31}$$

where $\hat{a}_k^{-1}$ and $\hat{a}_k^{\dagger -1}$ are one-sided inverse operators, $\mathbf{I}$ is the identity operator and $|0\rangle\langle 0|$ denotes the projection operator on the vacuum of the k-well. Such a projection, however, should be quite irrelevant in our case, given the limitations we have assumed on the subspace where the Hamiltonian (6) should be supposed to be acting upon, i.e., limited only to high occupation configurations. So, we will disregard in what follows the last term in (31), which in turn leads to a well-defined operator (29) that, combined with expressions (25) and (26), suggests that the following additional terms to the BH Hamiltonian (6) should be taken into account:

$$\hat{H}_1 = \frac{i\hbar I^0(t)}{2}\{\ln[\hat{a}_1^\dagger(t)\hat{a}_2(t)] - \ln[\hat{a}_2^\dagger(t)\hat{a}_1(t)]\} \tag{32}$$

$$\hat{H}_2 = -\frac{i\hbar}{2}\int_0^t \dot{I}^0(t')\{\ln[\hat{a}_1^\dagger(t')\hat{a}_2(t')] - \ln[\hat{a}_2^\dagger(t')\hat{a}_1(t')]\}dt'. \tag{33}$$

We may now rewrite the Heisenberg equation (12) in the case of moving barriers as,

$$\frac{d\hat{a}_k}{dt} = \frac{i}{\hbar}[\hat{H}_{BH} + \hat{H}_1 + \hat{H}_2, \hat{a}_k] + \frac{\partial \hat{a}_k}{\partial t}, \tag{34}$$

where the partial derivative denotes a time derivative of the Schrödinger operator, which next is time-evolved to reach the Heisenberg picture. To evaluate the commutator $[\hat{H}_1, \hat{a}_k]$ in (34), we make use of the following result [33],

$$[\hat{a}_k, \ln \hat{a}_k^\dagger] = \frac{\partial(\ln \hat{a}_k^\dagger)}{\partial \hat{a}_k^\dagger} = \hat{a}_k^{\dagger -1},$$

which yields,

$$\frac{i}{\hbar}[\hat{H}_1, \hat{a}_k] = -\frac{\dot{N}_k^0}{2}\, \hat{a}_k^{\dagger -1}. \tag{35}$$

On the other hand, to evaluate the partial derivative in (34) it is convenient, at a first stage, to do it in the limit (13). Then, we have in the Schrödinger picture, $(\hat{a}_k)_{\rm S} \to \sqrt{N_k^0(t)}\exp(i\phi_k^0)$, where only the population of the localized states will be time-dependent as barriers move. Therefore, the time derivative turns out to be,

$$\left(\frac{\partial \hat{a}_k}{\partial t}\right)_S \to \frac{\dot{N}_k^0}{2\sqrt{N_k^0}\exp(-i\phi_k^0)} \leftarrow \frac{\dot{N}_k^0}{2}(\hat{a}_k^{\dagger -1})_S, \tag{36}$$

which also turns out to arise from the limit (13) of the above right-hand side expression. Finally, turning to the Heisenberg representation in (36), we may conclude that the term of the partial time derivative in (34) and the term (35) cancel each other, yielding the following Heisenberg equation of motion,

$$\frac{d\hat{a}_k}{dt} = \frac{i}{\hbar}[\hat{H}_{BH} + \hat{H}_2, \hat{a}_k]. \tag{37}$$

Here an eventual calculation of the commutator $[\hat{H}_2, \hat{a}_k]$ in the above expression appears as a quite difficult task, as it involves the evaluation of commutators of Heisenberg operators at different times. However, according to (33) and (28), such a hysteretic contribution to the equation of motion should be negligible, except for accelerated or nearly overlapping barriers. Moreover, no evidence of a discrepancy between the experimental results for adiabatically accelerated barriers and the corresponding GP simulations has been reported so far [3, 10]. Thus, we will disregard in what follows any hysteretic contribution stemming from (26) or (33) to the energy and the equations of motion, both for GP simulations and the TM model. Finally to summarize, we will assume that the Heisenberg equation of motion remains formally equivalent to the original expression (12), except for the parameters of the BH Hamiltonian (6) that now become time-dependent as barriers move. The same occurs with the TM equations of motion (14) and (15), along with the effective interaction correction

(20). On the other hand, given that the energy represented by $\mathcal{H}$ in the Hamiltonian formalism (23) acquires for moving barriers the additional term (25), we may generalize Eqs. (23) as,

$$\hbar\Delta\dot{N}_2 = -\frac{\partial\mathcal{H}}{\partial\phi}\ ;\ \hbar\dot{\phi} = \frac{\partial\mathcal{H}}{\partial\Delta N_2}, \tag{38}$$

where now the Hamiltonian is given by $\mathcal{H} = \Delta E_{TM} + \hbar I^0\phi$, and ($\Delta N_2$,$\phi$) represent the canonically conjugate variables, with $\Delta N_2 = N_2 - N_2^0$. In addition, the potential energy of the "phase particle" in (24) becomes for moving barriers a "tilted washboard" potential [6–10, 26–28] given by,

$$\hbar I_c\left(1 - \cos\phi + \frac{I^0}{I_c}\phi\right), \tag{39}$$

with

$$I_c = \frac{N\Delta E}{2\hbar} \tag{40}$$

the so-called Josephson critical current. Here it is worthwhile noticing that all the currents we have defined so far, i.e., the particle current $I = \dot{N}_2$, the bias current $I^0 = \dot{N}_2^0$ and the critical current I_c, actually are twice the corresponding current across each JJ. The average slope of the "washboard" in (39) is proportional to the quotient I^0/I_c and the local extrema of such a potential arise from the Josephson current-phase relation [6–8, 34]

$$I^0 = -I_c\sin\phi. \tag{41}$$

Particularly, the stationary states for barriers at rest ($I^0 = 0$) located at $\phi = 0$ (minimum) and $\phi = \pm\pi$ (maximum) turn out to be displaced for moving barriers to the following locations,

$$\phi_m = -\sin^{-1}\left(\frac{I^0}{I_c}\right), \tag{42}$$

and

$$\phi_M = \sin^{-1}\left(\frac{I^0}{I_c}\right) - \frac{I^0}{|I^0|}\pi, \tag{43}$$

where ϕ_m and ϕ_M denote the phase differences of the minimum and maximum of the washboard potential within the interval $-\pi < \phi < \pi$, respectively. The above results can equivalently be expressed in terms of the barrier speed by means of Eq. (27),

$$\frac{I^0}{I_c} = \frac{f}{f_c}, \tag{44}$$

where $f = \dot{\theta}/(2\pi)$ denotes the barrier rotation frequency and

$$f_c = \frac{\Delta E}{h(\partial Z_0/\partial\theta)}, \tag{45}$$

represents the critical rotation frequency corresponding to the Josephson critical current (40). We may see from (42) and (44) that the phase particle can remain "trapped" around the potential minimum provided the bias current does not exceed the critical value I_c, or equivalently, the barrier speed remains below the critical frequency f_c. Such a dynamics, characterized by a bounded phase difference, vanishing average values for $\dot{\phi}$ and $\mu_2 - \mu_1$ (20), and a particle current that matches the bias current, corresponds to the so-called dc Josephson regime (analogous to the superconducting zero-voltage state [6–8]). Otherwise, for a bias current or a barrier speed above the critical values, the local extrema of the washboard potential disappear and the particle will "fall down" indefinitely, yielding a dynamics of running phase (nonvanishing values for $\langle\dot{\phi}\rangle$ and $\langle\mu_2-\mu_1\rangle$) and an alternating particle current. Such characteristics define the so-called ac Josephson regime, which is analogous to the superconducting nonzero-voltage state [6–8]. This regime can also be accessed from below the critical values, provided the energy of the particle $\mathcal{H}$ exceeds the maximum value of the potential to escape over the top of the barrier and propagate down the washboard. We disregard here any additional way of escaping, such as, by thermal activation at finite temperatures, or by a macroscopic quantum tunneling process [26, 27], given the small relative value of the plasma frequency ω_p in our case.

1. Energy landscape

Although the above heuristic model of a fictitious particle moving in the washboard potential may be useful to understand the dynamics of the phase within the different Josephson regimes, such a model is based on several approximations that eventually could lead to inaccuracies with respect to the GP simulation results. For instance, the term corresponding to the kinetic energy in (24) was derived from the equation (15), instead of the more accurate expression (20), in addition, the parameters of the kinetic energy and the washboard potential (39) may depend on the barrier position (see, e.g., Eqs. (27), (40) and Fig. 4), leading to a nonconserved energy that could eventually invalidate such a model. So, to avoid such shortcomings, we may utilize a more formal treatment which consists in studying the condensate energy landscape as a functional of the order parameter [35]. This in our case amounts to study the energy $\mathcal{H} = \Delta E_{TM} + \hbar I^0 \phi$ as a function of the phase difference and the particle imbalance. Previously we have seen that the condensate energy with barriers at

rest (22) presents a minimum for the ground-state $\phi = 0$ and a maximum (saddle) for the excited state $\phi = \pm\pi$, both for $Z = Z_0$. Now, by canceling the partial derivatives in (38), we may easily find such extrema for a general case of moving barriers. Thus, we encounter that the energy should present local extrema for $Z = Z_0 = 2N_2^0/N - 1$ and phase differences fulfilling the following equation,

$$I^0 = -I_c \sin\phi + (2NSN_2^0/\hbar)(1 - N_2^0/N)\sin 2\phi, \tag{46}$$

which, taking into account that the second harmonic contribution of the last term [28, 34] can be safely neglected for our condensate, becomes equivalent to the previously considered simple sinusoidal current-phase relation (41). Therefore, according to the sign of the second derivatives of $\mathcal{H}(\Delta N_2, \phi)$, there must be a minimum of the energy at $Z = Z_0$ and $\phi = \phi_m$ given by Eq. (42), and a saddle (minimum for Z and maximum for ϕ) at $Z = Z_0$ and $\phi = \phi_M$ given by Eq. (43). Particularly, the Z-dependence of the energy turns out to be quite simple since it is dominated by the harmonic term $\sim (Z - Z_0)^2$ in (22). So, we can obtain a full picture of the energy landscape by setting $Z = Z_0$ and analyzing the remaining dependence on the phase difference and the bias current, as depicted in Fig. 3. A typical system trajectory in the dc regime will reside in the vicinity of the dashed line, which corresponds to the phase difference at the energy minimum for each value of the bias current. On the other hand, the ac regime will be attained when exceeding the critical value of the bias current (or the barrier speed), as well as if the system acquires enough energy to overcome the saddle (solid) lines. We note that Fig. 3 can also be regarded as an energy landscape depending on the order parameter ϕ and the control parameter [35] $I^0/I_c = f/f_c$ (see Eqs. (44) and (45)), where the latter actually embodies two independent control parameters, the barrier position and its velocity. However, it will be seen in Fig. 4 that the dependence on the barrier position of I_c and f_c turns out to be very weak for $\theta \lesssim 0.3\pi$, so the problem within such an interval becomes reduced to the simplest one of a single control parameter (bias current I^0, or rotation frequency f). In fact, we display in Fig. 4 the Josephson critical current and the corresponding critical frequency as functions of the barrier position, where we may observe that they remain practically constant until the barriers begin to overlap each other, a process which eventually may cause them to drop toward vanishing values. On the other hand, the inset of such a figure shows the domains of the dc and ac Josephson regimes on a phase versus bias current (or rotation frequency)

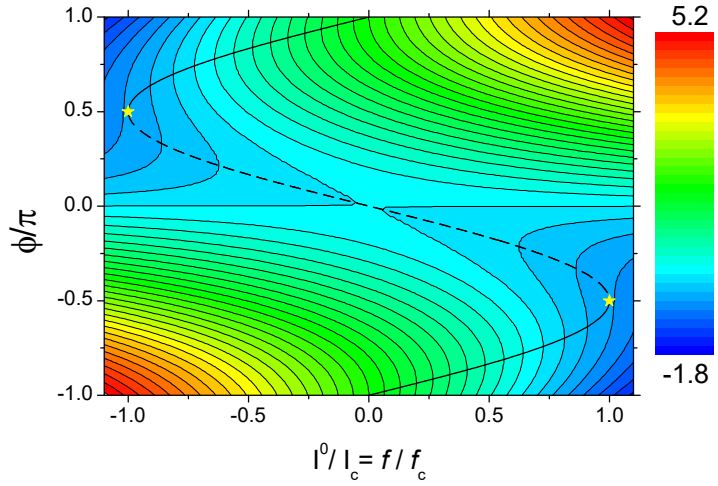

FIG. 3. Energy landscape for $Z = Z_0$. The color scale corresponds to the adimensionalized energy $(\Delta E_{TM} + \hbar I^0 \phi)/\hbar I_c$, while the dashed (solid) line locates its minimum (saddle) for each value of the bias current or barrier rotation frequency. The yellow stars indicate the critical points where minimum and saddle coalesce.

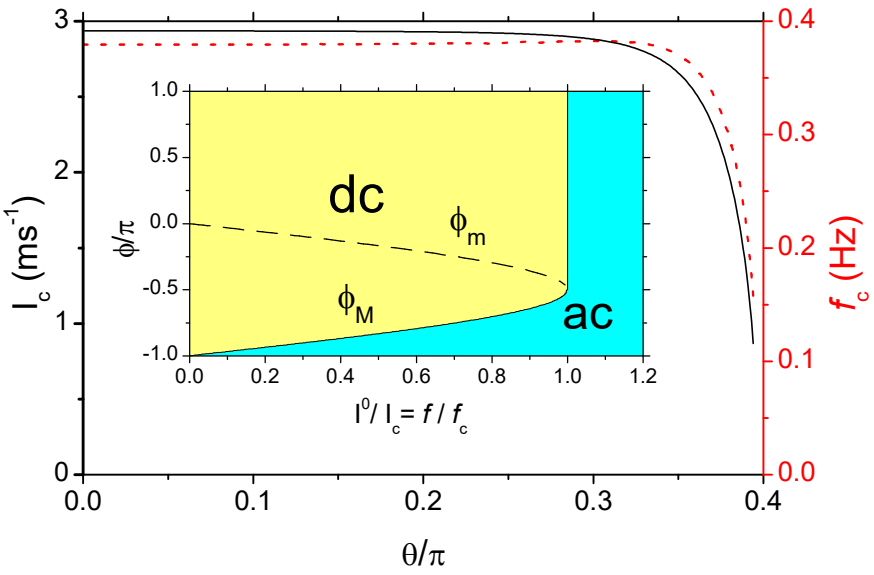

FIG. 4. Josephson critical current I_c (Eq. (40), solid line) and critical frequency f_c (Eq. (45), dotted line) versus the barrier position θ. Inset: the dc (ac) Josephson regime corresponds to bias currents or barrier frequencies below (above) the critical values. Particularly, the ac domain extends below the critical values for phase differences beyond that of the energy saddle ϕ_M (Eq. (43)). On the other hand, the phase difference ϕ_m (Eq. (42)) of the energy minimum is depicted as a dashed line.

diagram. We note that according to Fig. 3 a straightforward extension of such a diagram to negative abscissas could be easily depicted.

2. Adiabatic barrier motion: dc-ac transition and hysteretic phenomena

Starting from an initial condition with the barriers at rest and the condensate in the ground state, any barrier motion will trigger an oscillation of the order parameter, in particular, the particle current and the phase difference, which for small amplitudes will be ruled by the plasma frequency ω_p. However, since we are interested in the dc to ac transition driven by a current bias, and being the departure of the actual current from the bias current one of the main signatures of such a transition, one should try to suppress, or at least minimize, such oscillations, as they could certainly interfere with our observations. To this aim, we have assumed the following barrier trajectory that preserves the continuity of the acceleration $\ddot{\theta}$ along the whole path,

$$\theta(t) = -\frac{\theta(0)}{\pi}[\sin(\omega t + \pi) + \omega t - \pi], \quad \omega = -\frac{\pi^2 f_{\max}}{\theta(0)}, \tag{47}$$

where $f_{\max}$ denotes the maximum value of the rotation frequency $f = \dot{\theta}/(2\pi)$ that may be regarded as a control parameter of the approach to the dc-ac transition. For instance, for $f_{\max} > f_c$ we have that such a transition will certainly be reached during the trajectory. On the other hand, in order to reduce the angular frequency ω in (47), increasing the adiabaticity, we will assume a large value of the initial angle $|\theta(0)|$ compatible with nonoverlapping barriers, namely $\theta(0) = -0.394\pi$. We depict in Fig. 5 the rotation frequency $f = \dot{\theta}/(2\pi)$ versus time, as well as its dependence on the barrier position itself. We have considered two kinds of trajectories. In the first one, the barriers are adiabatically accelerated according to (47) until reaching the maximum velocity with $f = f(\theta = 0) = f_{\max}$ at $\omega t = \pi$ (Fig. 5), from where they maintain such a velocity. Such trajectories are primarily intended to study the behavior of the condensate under a uniform barrier velocity. Note that according to (27) we have $I^0 = N\pi(\partial Z_0/\partial\theta)f$, so a uniform barrier velocity will keep the current bias also uniform, except for nearly overlapping barriers (see Fig. 2). Moreover, under such conditions we could approximate $I^0(\theta)/I^0(\theta = 0) \simeq f(\theta)/f(\theta = 0)$, from which we may conclude that the ordinate of Fig. 5 can also be regarded as the bias current $I^0/I^0_{\max}$. We depict in Fig. 6 the GP simulation results for the time evolution of the particle current for a

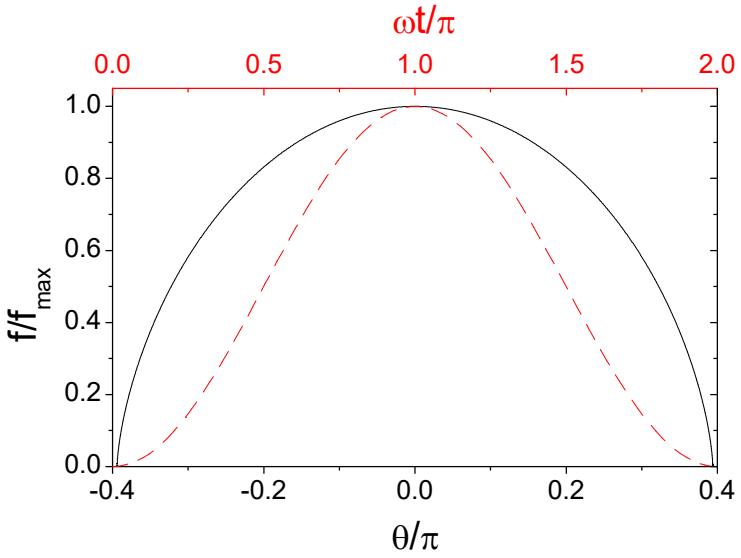

FIG. 5. Adiabatic barrier motion. Time evolution of the barrier rotation frequency $f = \dot{\theta}/(2\pi)$ arising from Eq. (47) in units of its maximum value $f_{\max} = f(\theta = 0)$ (dashed line), and the same quantity versus the barrier position θ (solid line).

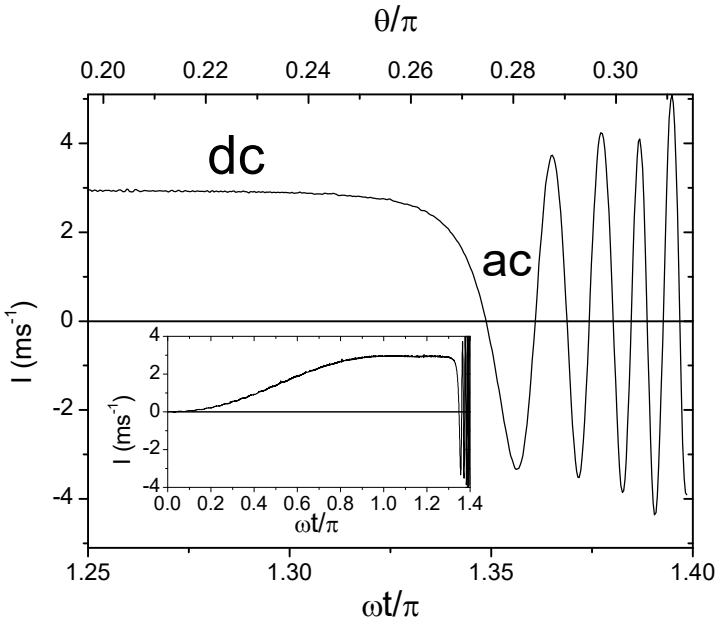

FIG. 6. GP simulation results for the time evolution of the particle current for the barrier trajectory (47) with $f_{\max} = 0.38$ Hz and maintaining the maximum barrier speed for $\omega t > \pi$. The main plot shows the dc to ac transition that occurs when $f_c(\theta(t))$ drops below $f_{\max}$ (cf Fig. 4), with $\theta(t)$ given in the top abscissa. The inset shows the particle current for the complete barrier trajectory.

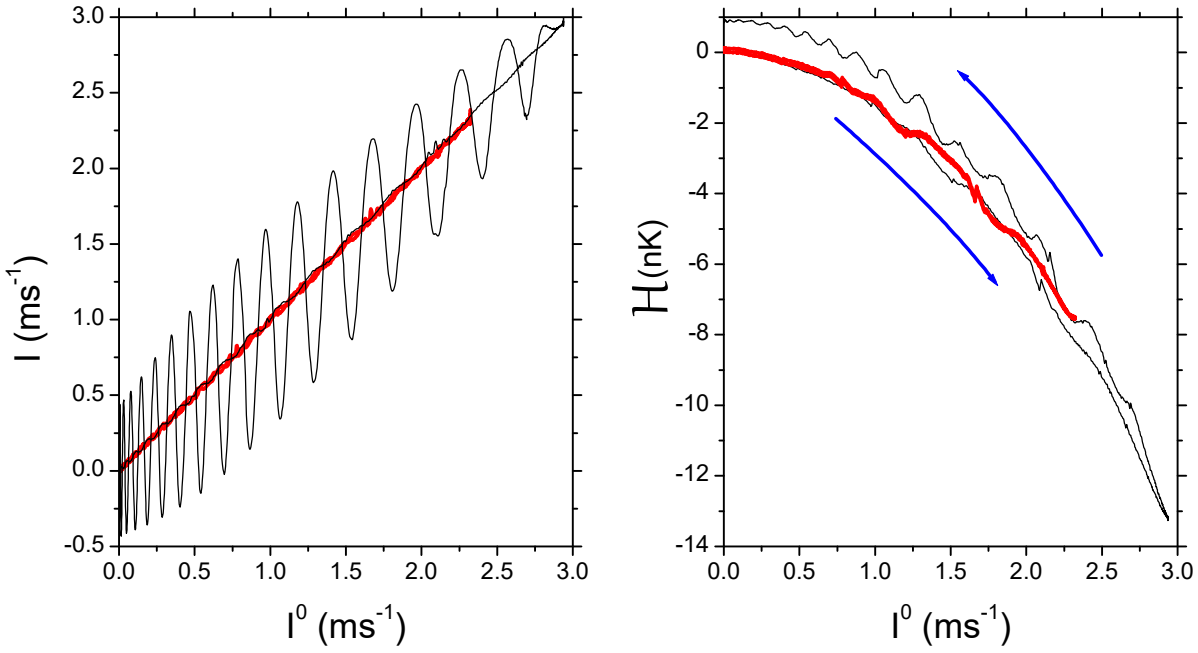

FIG. 7. Left panel: GP simulation results for the particle current versus bias current (I vs I^0) paths for the symmetric barrier trajectories of Fig. 5. The non-hysteretic path corresponding to $f_{\max} = 0.3$ Hz is depicted by the thick (red) solid line, while the hysteresis loop corresponding to $f_{\max} = 0.3815$ Hz is represented by the thin (black) solid line. Right panel: same paths for the energy $\mathcal{H} = \Delta E_{TM} + \hbar I^0 \phi$, where the blue arrows indicate the path directions.

barrier trajectory of this kind with $f_{\max} = 0.38$ Hz. We may observe the dc to ac transition, which occurs, despite of the fixed value of the bias current (plateau of the inset in Fig. 6), due to the dependence of the critical current on the barrier angle, as shown in Fig. 4.

The other kind of barrier trajectories, corresponding to the symmetric curves of Fig. 5, turns out to be particularly useful to observe hysteresis. We first note that the maximum bias current for such trajectories (maximum barrier speed in Fig. 5) occurs for $\theta = 0$, with a critical current slightly below 3 ms^{-1} and a critical rotation frequency obtained from GP simulations of about 0.382 Hz (Fig. 4). Hysteretic and non-hysteretic evolutions are clearly represented in the particle current versus bias current graph shown in Fig. 7. In fact, we may see that for a barrier trajectory with $f_{\max} = 0.3$ Hz, well below the critical value, the particle current follows exactly the bias current for the whole path, except for the low amplitude (plasma) oscillations. On the other hand, for $f_{\max} = 0.3815$ Hz, although the particle current matches again the bias current for the first half of the path, once the bias

current reaches its maximum close to the critical current, it gives rise to a quite hysteretic loop with large amplitude oscillations of the particle current. In the right panel of Fig. 7, we may see a similar behavior for the energy, since for the barrier trajectory with $f_{\max} = 0.3$ Hz, we have fully overlapped paths for increasing and decreasing bias currents, while for $f_{\max} = 0.3815$ Hz, such energy paths become split, yielding a way back with a higher energy, which stems from the above oscillations of the particle current. However, such hysteretic effects may be difficult to observe in practice due to the requirement of an extremely fine tuning of the barrier velocity close to the critical value. A more favorable scenario for the hysteresis observation could take place for a barrier trajectory (47) with $f_{\max} > f_c$, along with the presence of a resistive flow in the ac regime able to bring the condensate back to the dc domain. In addition to the effect of noncondensed atoms in a thermal component, such resistive flows may arise from quantum phase slips corresponding to vortices created within the barrier and shed into the superfluid [11, 36]. In any case, we may analyze such a scenario by considering a suitable circuit analogy. It is worth mentioning in this respect, that as a basic representation of the wide interrelation between electronics and atomtronics [37], simple models of electronic circuitry have been shown to capture the essential physics of superfluid transport in ultracold gases [38–40]. Particularly, the RCSJ model [19], which consists in a very simple equivalent circuit proven to be exceptionally successful in modeling the dynamics of superconducting Josephson devices [6–8, 26, 27], has also been shown to yield similarly good results for the dc and ac Josephson effects in ultracold gases [9, 10, 28]. The RCSJ equivalent circuit for a JJ is composed of three parallel elements: a shunt resistance R, a shunt capacitance C and a pure Josephson element that works as a nonlinear inductance [8, 41]. Thus, Kirchhoff's law corresponds in our case to $I^0 = I_s + I_n + I_d$, where the bias current I^0 yields the three parallel currents: the superfluid current $I_s = -I_c \sin\phi$, the normal ohmic current $I_n = -G\Delta\mu$ and the displacement current $I_d = -Cd(\Delta\mu)/dt$, being $G = 1/R$ the conductance and

$$\begin{aligned} \Delta\mu &= \hbar d\phi/dt \\ &= \Delta N_2/C, \end{aligned} \tag{48}$$

where the first line (cf. Eq. (20)) corresponds to the general voltage-phase relation of the Josephson effect and the second line corresponds to the definition of the capacitance C as the ratio of the particle number difference from the equilibrium value $\Delta N_2 = N_2 - N_2^0 =$

$N(Z - Z_0)/2$ and the chemical potential difference $\Delta\mu = \mu_2 - \mu_1$. Now, replacing the displacement current according to (48) in Kirchhoff's law we obtain,

$$I = I_s + I_n, \tag{49}$$

where $I = N\dot{Z}/2 = \dot{N}_2$ denotes the particle current flowing from well '1' to well '2' (Fig. 1). Equation (49) tells us that such a particle current consists of a superfluid component I_s and a normal component $I_n = -\Delta\mu/R$, which will only be nonnegligible for the finite chemical potential differences of the ac regime. As regards the superfluid current $I_s = -I_c \sin\phi$, we may obtain the expression of the Josephson inductance L_J from the time derivative $dI_s/dt = -I_c \cos\phi\, \Delta\mu/\hbar = -\Delta\mu/L_J$, which yields the phase-dependent expression $L_J = \hbar/(I_c \cos\phi)$ [8, 41].

Although the RCSJ model accurately describes the experimental results in cold gases, some parameters of the model are obtained by fitting the data and lack of a rigorous derivation. So, a detailed comparison with the more fundamental TM model should be relevant in this respect. To this aim, we first compare Eq. (48) with the TM equation (20), from which we may immediately obtain the following expression for the capacitance

$$C = \frac{1}{2(U + BZ)}, \tag{50}$$

which jointly with the Josephson inductance L_J constitute an LC oscillator at the frequency $1/\sqrt{L_J C}$, whose low amplitude limit ($\phi \simeq 0$ and $Z \simeq Z_0$) yields the more accurate expression $\omega_p = \sqrt{2I_c(U + BZ_0)/\hbar}$ for the plasma frequency than that given at the end of Sec. III A. On the other hand, if one approximates the TM equation (14) for $Z \simeq Z_0$ and neglects the term proportional to the second order hopping parameter S, one obtains $N\dot{Z}/2 = -I_c \sin\phi$, which just corresponds to the Eq. (49) in the dc regime. As regards the normal component I_n, it is absent from our TM model, since it stems from a formalism without any assumption about dissipative channels. The simplest way of including such dissipative effects would consist in adding to the right-hand side of Eq. (14) a term proportional to the RCSJ normal current $-G\Delta\mu$, along with a phenomenological value of the conductance G [20]. More elaborate procedures that quantitatively take into account the effect of damping at a finite temperature could be carried out by resorting to a stochastic projected GP equation [42]. We depict in Fig. 8 the results of the above simple version of a damped TM model for a symmetric barrier trajectory with $f_{\max} = 0.42$ Hz above the critical value and two values

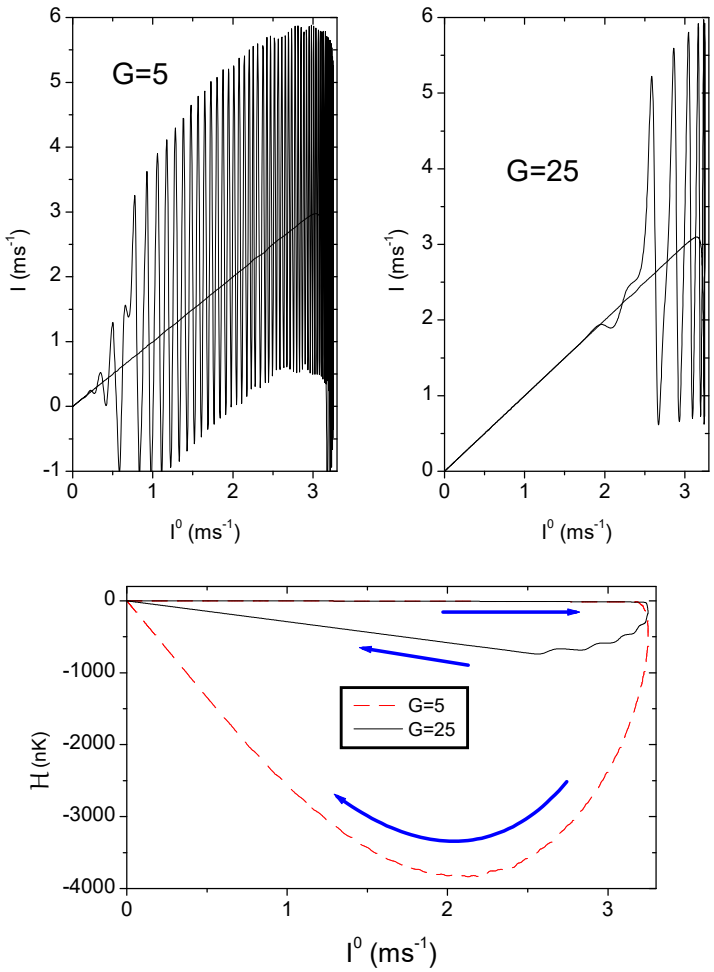

FIG. 8. Same as Fig. 7 for the results arising from a damped TM model with $f_{\max} = 0.42$ Hz and two values of the conductance G (in units of $\hbar^{-1}$).

of the conductance. We observe that the particle current follows the increasing values of the bias current up to the critical point, from where it begins to display oscillations of a higher amplitude than those observed in Fig. 7. Such oscillations, which correspond to a dynamics within the ac regime, persist with the decreasing bias current up to a value which marks the reentrance to the dc regime. This behavior turns out to be analogous to the phenomenon of a return or 'retrapping' current in a hysteretic superconducting JJ, occurring when the junction switches back from the voltage state to the zero-voltage state [17, 18]. Although such an ac to dc transition is common in superconducting systems, we are not aware of any observation of this kind in a BEC. As depicted in Fig. 8, such a return current grows with the conductance, leading for high values of G to an overdamped

and quasi-non-hysteretic motion. In contrast, low conductances with small return currents yield longer evolutions within the ac regime and, hence, quite hysteretic processes. It is interesting to relate hysteresis with the energy evolutions depicted in Figs. 7 and 8. On the one hand, the system dynamics driven by the barrier trajectory with $f_{\max} = 0.3815$ Hz in Fig. 7, which entirely takes place within the dc regime, develops by performing a round trip that travels twice the same line of minima of the energy landscape (Figs. 3 and 4), with hysteretic effects stemming from the oscillations around such minima developed during the return path. In contrast, the evolutions depicted in Fig. 8 correspond to the more common hysteresis scenario which involves more than a single minimum of the energy landscape [35]. In fact, for increasing bias currents up to the critical value, the system travels the above line of energy minima ending at the critical point $I^0 = I_c$ in Fig. 3. Then, the system leaves the dc regime and entering the ac domain, there is an onset of a 'running down hill' process due to the absence of any local energy minimum. Next, following the subsequent barrier trajectory, the decreasing bias current falls again below the critical value with a reappearance of local energy minima and the possibility for the system to be 'retrapped' and thus able to return to the dc domain and travel a different line of minima than that left after entering the ac regime. We depict in the lower panel of Fig. 8 the hysteresis loops performed by the energy versus bias current trajectories for two values of the conductance G. Note that the smaller the conductance, the deeper energy fall occurring as the system remains in the ac regime. However, for conductance values below certain threshold, the return to the dc domain does not occur, and in the final configuration of a vanishing bias current (barriers at rest), the system ends in a high-energy nonequilibrium self-trapped state, with a quite compressed condensate at site 1 (Fig. 1) [3, 11, 14]. Finally, we remark that it would be interesting to generate experimental results about the return transition from ac to dc, which would allow to test the validity of the above predictions of the damped TM model.

3. GP simulations and comparison to TM model results

We have studied the transition from the dc to the ac regime for different barrier trajectories and initial states of the system. Unless stated, we will assume an initial condensate in equilibrium at the ground state. First we will consider the evolution for a uniform barrier velocity after the initial adiabatic acceleration. We depict in Fig. 9 the phase difference

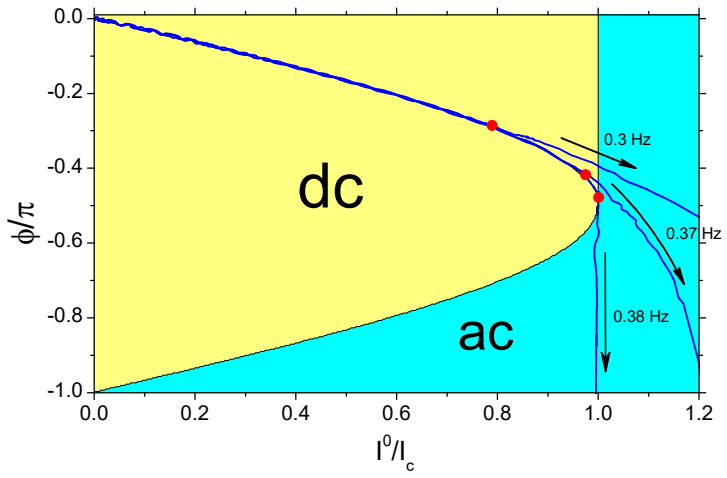

FIG. 9. Phase difference versus bias current from GP simulation results for three barrier trajectories (47) with constant values of 0.3, 0.37 and 0.38 Hz of the barrier rotation frequency from the corresponding red dots.

versus bias current for three values of the final barrier velocity. We may observe that the system travels quite closely the line of energy minima (Fig. 4, inset) up to reaching the uniform rotation frequency (red dots). Then, the subsequent evolution in the dc regime is represented by the red dots in Fig. 9, since the condensate stays with a constant phase difference and a uniform particle/bias current. Finally, a sudden transition to the ac regime occurs when the Josephson critical current becomes smaller than the particle/bias current for the increasing barrier angles (Fig. 4). In fact, the top panel of Fig. 10 displays such a behavior for the particle currents corresponding to the barrier trajectories with $f_{\max} = 0.3$ Hz and $f_{\max} = 0.37$ Hz, while the bottom panel also shows that the critical condition for the barrier rotation frequency $f = f_c$ happens quite simultaneously with the critical crossings $I = I_c$ in the top panel. On the other hand, the case $f_{\max} = 0.38$ Hz shows important differences with respect to those of the lower rotation frequencies. We notice in Fig. 10 that the steady particle current for $\theta > 0$ obtained from the GP simulation, as well as the rotation frequency 0.38 Hz, practically coincide with the critical values arising from the TM model for $\theta/\pi \lesssim 0.2$. Thus, it is easy to understand that under such conditions the model should not be expected to yield accurate results for the barrier angle at which the transition should occur.

In Fig. 11, we may appreciate the way in which such a transition is reflected on the

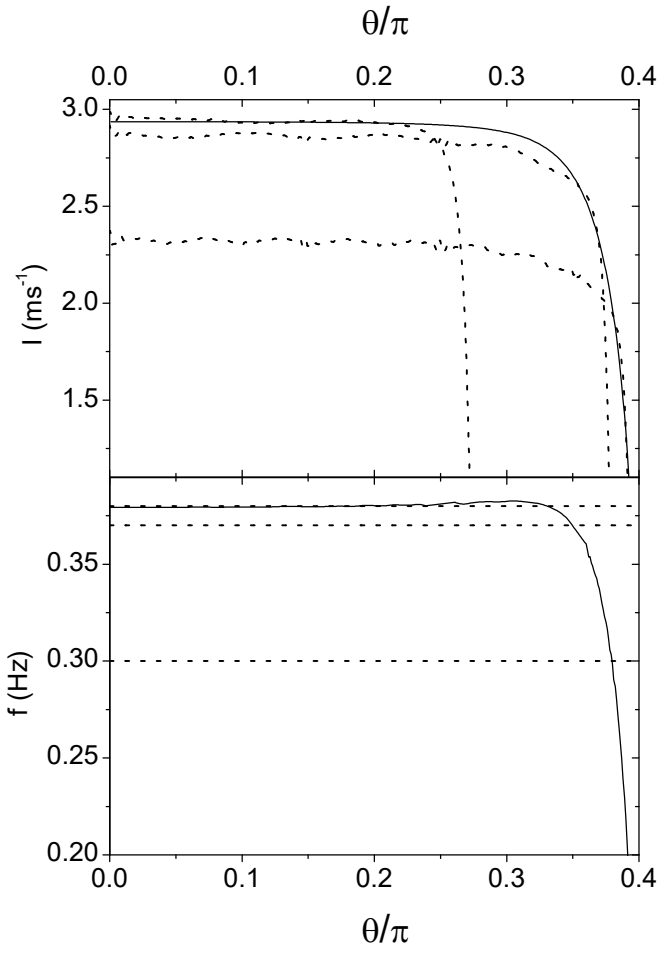

FIG. 10. Top panel: critical current I_c versus the barrier angle θ (solid line) and particle currents arising from GP simulations (dotted lines) for the barrier trajectories of Fig. 9 with the uniform rotation frequencies 0.38, 0.37 and 0.3 Hz attained from $\theta = 0$ with, respectively, top to bottom intersections with the ordinate and left to right intersections with the abscissa. The flow oscillations of the ac regime have not been displayed for clarity. Bottom panel: same as top panel for the critical rotation frequency f_c (solid line) as compared to the rotation frequencies 0.38, 0.37 and 0.3 Hz (dotted lines) from top to bottom, respectively.

condensate evolution with the highest rotation frequency $f_{\max} = 0.38$ Hz of Fig. 9. In addition to the plain dc-ac current transition already shown in Fig. 6, we may observe that the remaining condensate observables show quite sharp variations at the transition. In fact, the sudden compression undergone by the condensate at site 1, along with the corresponding expansion at site 2, becomes reflected in the top panel of Fig. 11 through the sharp decrease

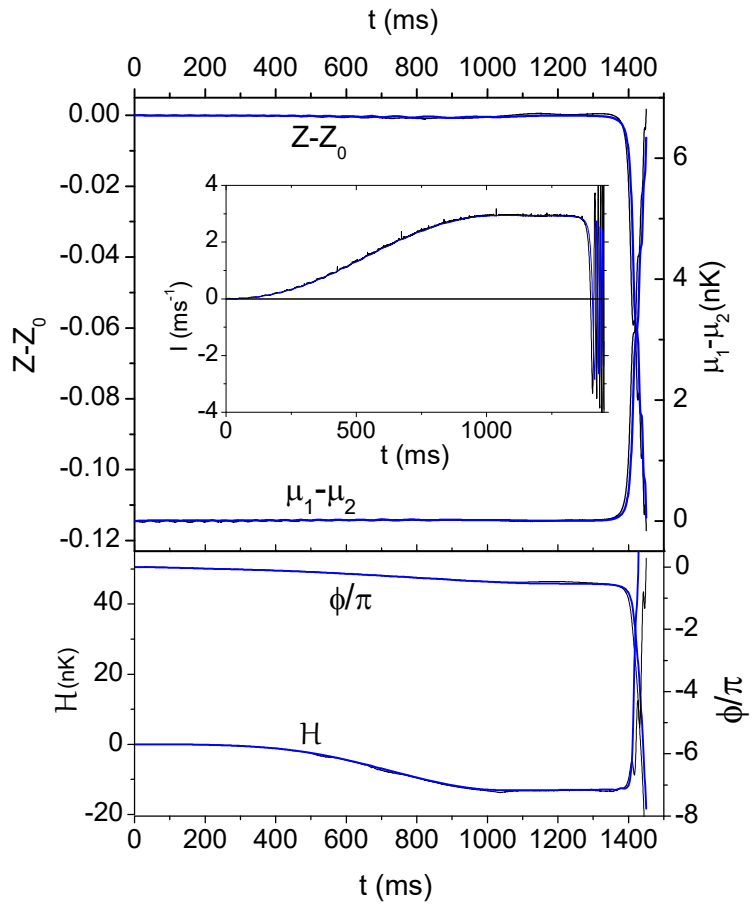

FIG. 11. Time evolution of the imbalance departure from the equilibrium value $Z - Z_0$, chemical potencial difference $\mu_1 - \mu_2$, particle current I (inset), phase difference ϕ, and energy $\mathcal{H}$ from GP simulation results (black solid lines) for the barrier motion with a maximum rotation frequency $f_{\max} = 0.38$ Hz referred to in Figs. 6, 9 and 10. The blue solid lines represent the corresponding TM model results with a best fit value of $f_{\max} = 0.37862$ Hz.

(increase) of the imbalance departure from the equilibrium value $Z - Z_0$ (chemical potential difference $\mu_1 - \mu_2$) at the transition from the almost vanishing values shown in the dc regime. On the other hand, the bottom panel of Fig. 11 shows that after the adiabatic barrier acceleration (below 1000 ms), the phase difference and the energy remain constant up to the transition to the ac regime, which is characterized by a running downwards phase difference and an energy jump stemming from the sudden compression/expansion of the condensate that triggers the term $\sim (Z - Z_0)^2$ in (22). Here it is important to remark the excellent agreement that show in Fig. 11 the GP simulation results and the corresponding

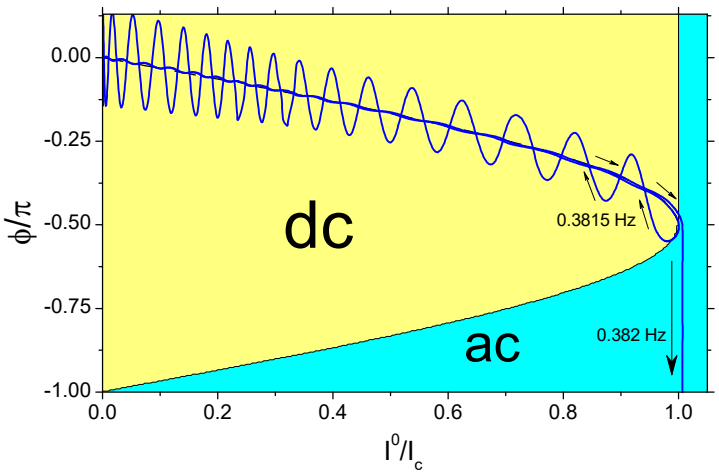

FIG. 12. GP simulation results for the phase difference versus bias current for two symmetric barrier trajectories (Fig. 5) with $f_{\max} = 0.3815$ Hz and $f_{\max} = 0.382$ Hz.

TM results for a slightly modified best fit value of the maximum rotation frequency (less than 0.4%), with respect to that of the GP simulation.

The condensate evolution for two slightly different symmetric trajectories of the barriers is depicted in Fig. 12. Here the faster trajectory with $f_{\max} = 0.382$ Hz provokes the condensate transition to the ac regime, while the slower trajectory ($f_{\max} = 0.3815$ Hz) yields the hysteretic loop within the dc domain, already seen in Fig. 7. It is interesting to observe in Fig. 12 that both trajectories in the phase difference versus bias current plane share the first part of the path, as they travel the line of energy minima up to the critical point, where minimum and saddle coalesce. At this point the condensate driven by the faster barriers 'drops' to the ac domain, while that driven by the slower barriers go a little further along the line of energy saddles. Note in Fig. 12 that this is precisely the fact that makes the return path (decreasing bias currents) oscillate around the line of energy minima. In other words, such a 'tour' beyond the critical point should be regarded as the source of the hysteretic behavior. To pursue with the study of this case, we depict in Fig. 13 time evolutions of the phase difference, particle current and energy that complement what represented in Figs. 7 and 12. Again, an excellent agreement between GP simulation and TM results is obtained with a slightly less best fit value of the maximum rotation frequency for the TM model (0.5%).

Finally, we will consider a different initial condition from that previously assumed of the

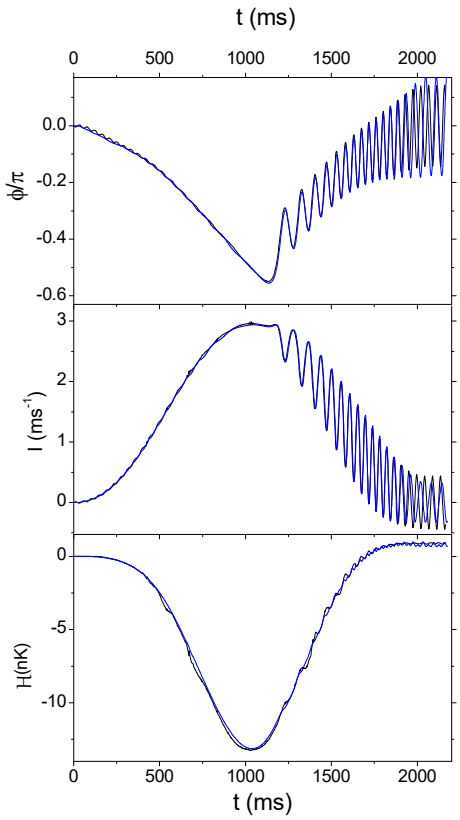

FIG. 13. Time evolution of the phase difference ϕ, particle current I and energy $\mathcal{H}$ from GP simulation results (black solid lines) and TM model results (blue solid lines) for symmetric barrier trajectories (Fig. 5) almost touching the critical point, with $f_{\max} = 0.3815$ Hz (GP simulation) and $f_{\max} = 0.37958$ Hz (TM model).

ground state of the condensate. In fact, we will assume an initial order parameter of the form $\psi_1 e^{i\phi} + \psi_2$, with ψ_j denoting the wavefunction of the localized state on the j-well and the parameter ϕ serving to introduce an initial phase difference between both wells. Note that $\phi = 0$ corresponds to the ground-state order parameter. Then, assuming again symmetric barrier trajectories, with $f_{\max} < f_c$ in this case, there will be a nonvanishing critical value of the initial phase difference above which the system will make the transition to the ac regime. In fact, we depict in Fig. 14 the GP simulation results for two initial phase differences just above and below such a critical value for a barrier trajectory with $f_{\max} = 0.3$ Hz. Thus, we may see overlapping phase differences for both initial conditions at increasing bias currents, yielding a trajectory of oscillations around the line of energy minima up to reaching the maximum rotation frequency (bias current). Next, the trajectories split into a returning

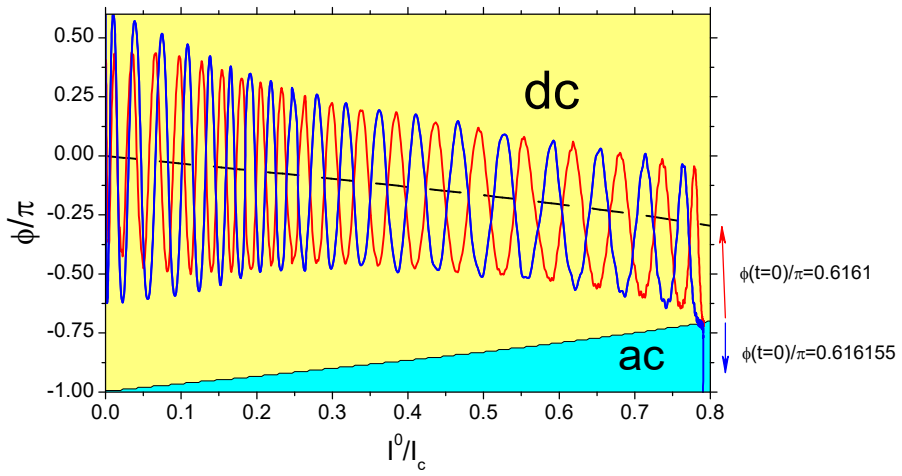

FIG. 14. Phase difference versus bias current from GP simulation results for two symmetric barrier trajectories (Fig. 5) with $f_{\max} = 0.3$ Hz and nonvanishing initial phase differences of 0.6161π and 0.616155π. Both curves turn out to be undistinguishable within the plot scale up to the maximum bias current, from where the return path for the former is depicted with the red solid line, while the latter conserves the original trace. The dashed line corresponds to the phase difference ϕ_m of the energy minimum.

oscillating path, similar to that developed for increasing bias currents (except for a phase displacement of π, approximately), and, for the higher initial phase difference, a trajectory that makes the transition to ac across the line of energy saddles. In Fig. 15, we depict the time evolution of the phase difference and the imbalance departure from the equilibrium value for the above configurations, where a very good agreement is observed between the GP simulation results and the TM model results with slightly higher best fit values of the initial phase differences ($\sim 1\%$).

IV. CONCLUSION

We have analized the effects of the barrier motion on the BH Hamiltonian and the equations of motion of an atom dc-SQUID. We have found that a couple of terms arising from the additional particle flow induced by the barriers displacement should be added to the condensate energy. In fact, in addition to the well-known contribution proportional to the bias current and the phase difference, which yields the tilting of the washboard potential,

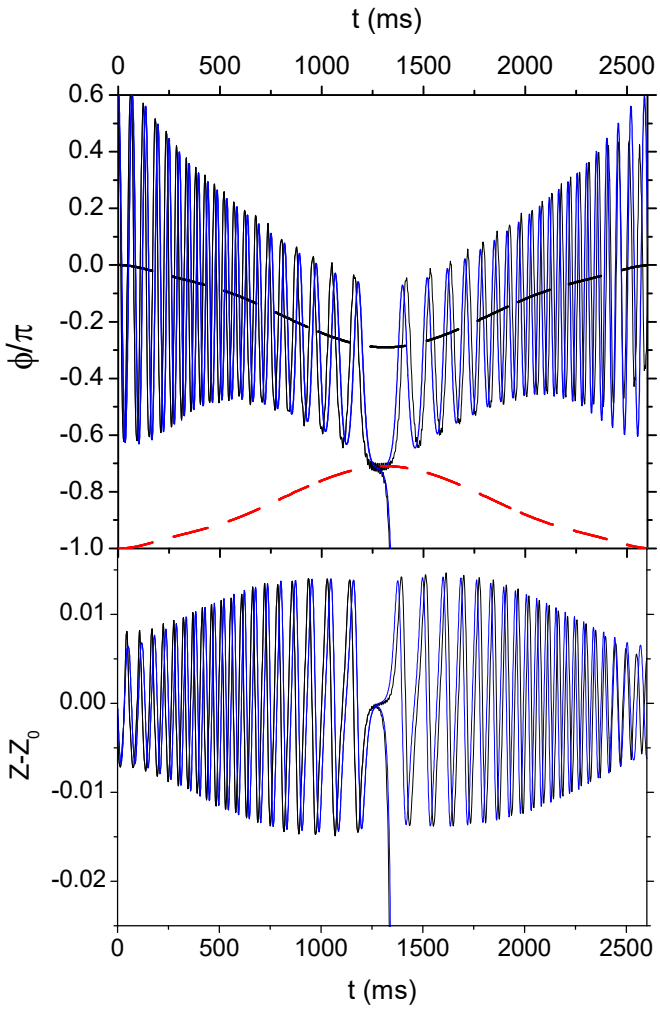

FIG. 15. Same as Fig. 14 for the time evolution of the phase difference ϕ and the imbalance departure from the equilibrium value $Z - Z_0$ (black solid lines). The blue solid lines depict the corresponding TM model results for initial phase differences of 0.6245π and 0.6248π, while the black (red) dashed line corresponds to the phase difference ϕ_m (ϕ_M) of the energy minimum (saddle).

we have identified a hysteretic term that should be considered for accelerated or overlapping barriers. Based on such energies, we have proposed two corresponding additional contributions to the BH Hamiltonian and have analyzed their effects on the Heisenberg equation of motion for the boson field operator in the TM approximation. Thus, we have found that the nonhysteretic additional contribution to the Heisenberg equation does cancel with that arising from the time derivative of the boson field operator in the Schrödinger representation, whereas the hysteretic contribution seems to be negligible in the present case of adiabatic barrier accelerations, according to the experimental results. So, we have utilized

formally the same GP and TM model equations derived for barriers at rest, except for the time dependence of parameters due to the barrier motion. By deriving the expression of the condensate energy from the BH Hamiltonian, we have studied the energy landscape as a function of an order parameter (phase difference) and a control parameter (bias current), determining the diagram with the location of dc and ac regimes. In addition, we have found that the Josephson critical current, and correspondingly the critical barrier speed, depend on the barrier position, a fact that makes that a dc to ac transition could always be reached for any uniform barrier velocity attained after the initial adiabatic acceleration. On the other hand, we have studied the condensate evolution driven by barrier trajectories symmetric with respect to the symmetric configuration of the dc-SQUID. Particularly, we analyzed the hysteretic effects stemming from a trajectory that almost reaches the critical point and develops an oscillating return within the dc domain, as compared to a sligthly faster trajectory that yields the condensate transition to the ac regime. In addition, we discussed an easier to detect hysteresis scenario that could arise for a sufficiently resistive flow in the ac regime. We have also seen that when the initial condensate presents a phase difference between both wells, instead of the ground state, there exists a critical value of such a phase difference above which the dc-SQUID makes a transition to the ac regime, irrespective of the maximum value of the barrier velocity attained at the symmetric trajectory. To conclude, we may remark that the excellent agreement between the GP simulation results and the TM model results found in all cases, leaves a good open window to further apply such a model and its corresponding BH Hamiltonian in order to gain better insights about this kind of critical phenomena.

ACKNOWLEDGMENTS

This work was supported by grants PIP 11220150100442CO from CONICET and UBA-CyT 20020150100157 from Universidad de Buenos Aires. Helpful discussions with D. M. Jezek are gratefully acknowledged.

---

[1] J. Clarke and A. I. Braginski, *The SQUID Handbook* (Wiley-VCH, Weinheim, 2004).

[2] Y. Sato and R. E. Packard, Rep. Prog. Phys. **75**, 016401 (2012).

[3] C. Ryu, P. W. Blackburn, A. A. Blinova, and M. G. Boshier, Phys. Rev. Lett. **111**, 205301 (2013).

[4] Y. Sato, Physics **6**, 123 (2013).

[5] C. A. Sackett, Nature **505**, 166 (2014).

[6] A. Barone and G. Paternò, *Physics and Applications of the Josephson Effect* (John Wiley, New York, 1982).

[7] M. Tinkham, *Introduction to Superconductivity*, 2nd ed. (McGraw-Hill, New York, 1996).

[8] R. Gross, A. Marx, and F. Deppe, *Applied Superconductivity: Josephson Effect and Superconducting Electronics*, De Gruyter Textbook Series (Walter De Gruyter, Berlin, 2016).

[9] S. Giovanazzi, A. Smerzi, and S. Fantoni, Phys. Rev. Lett. **84**, 4521 (2000).

[10] S. Levy, E. Lahoud, I. Shomroni, and J. Steinhauer, Nature **449**, 579 (2007).

[11] F. Jendrzejewski, S. Eckel, N. Murray, C. Lanier, M. Edwards, C. J. Lobb, and G. K. Campbell, Phys. Rev. Lett. **113**, 045305 (2014).

[12] K. C. Wright, R. B. Blakestad, C. J. Lobb, W. D. Phillips, and G. K. Campbell, Phys. Rev. Lett. **110**, 025302 (2013).

[13] S. Eckel, J. G. Lee, F. Jendrzejewski, N. Murray, C. W. Clark, C. J. Lobb, W. D. Phillips, M. Edwards, and G. K. Campbell, Nature **506**, 200 (2014).

[14] H. M. Cataldo and D. M. Jezek, Phys. Rev. A **90**, 043610 (2014).

[15] D. M. Jezek, P. Capuzzi, and H. M. Cataldo, Phys. Rev. A **87**, 053625 (2013).

[16] D. M. Jezek and H. M. Cataldo, Phys. Rev. A **88**, 013636 (2013).

[17] R. L. Kautz and J. M. Martinis, Phys. Rev. B **42**, 9903 (1990).

[18] M. G. Castellano, G. Torrioli, F. Chiarello, C. Cosmelli, and P. Carelli, J. Appl. Phys. **86**, 6405 (1999).

[19] W. C. Stewart, Appl. Phys. Lett. **12**, 277 (1968); D. E. McCumber, J. Appl. Phys. **39**, 3113 (1968).

[20] I. Marino, S. Raghavan, S. Fantoni, S. R. Shenoy, and A. Smerzi, Phys. Rev. A **60**, 487 (1999).

[21] E. M. Wright, J. Arlt, and K. Dholakia, Phys. Rev. A **63**, 013608 (2000).

[22] Y. Castin and R. Dum, Eur. Phys. J. D **7**, 399 (1999).

[23] P. Muruganandam and S. K. Adhikari, Comput. Phys. Commun. **180**, 1888 (2009).

[24] H. M. Cataldo and D. M. Jezek, Phys. Rev. A **84**, 013602 (2011).

[25] O. Dutta, M. Gajda, P. Hauke, M. Lewenstein, D.-S. Lühmann, B. A. Malomed, T. Sowiński, and J. Zakrzewski, Rep. Prog. Phys. **78**, 066001 (2015).

[26] J. Clarke, A. Cleland, M. Devoret, D. Esteve, and J. Martinis, Science **239**, 992 (1988).

[27] J. A. Blackburn, M. Cirillo, and N. Grønbech-Jensen, Phys. Rep. **611**, 1 (2016).

[28] W. J. Kwon, G. Del Pace, R. Panza, M. Inguscio, W. Zwerger, M. Zaccanti, F. Scazza, and G. Roati, (2019), arXiv:1908.09696 [cond-mat.quant-gas].

[29] S. M. Barnett and J. A. Vaccaro, eds., *The Quantum Phase Operator: A Review* (Taylor & Francis, New York, 2007).

[30] N. J. Higham, *Functions of Matrices: Theory and Computation* (SIAM, Philadelphia, 2008).

[31] L. Susskind and J. Glogower, Physics **1**, 49 (1964).

[32] C. L. Mehta, A. K. Roy, and G. M. Saxena, Phys. Rev. A **46**, 1565 (1992).

[33] M. K. Transtrum and J.-F. S. Van Huele, J. Math. Phys. **46**, 063510 (2005).

[34] A. A. Golubov, M. Y. Kupriyanov, and E. Il'ichev, Rev. Mod. Phys. **76**, 411 (2004).

[35] E. J. Mueller, Phys. Rev. A **66**, 063603 (2002).

[36] K. Xhani, E. Neri, L. Galantucci, F. Scazza, A. Burchianti, K.-L. Lee, C. F. Barenghi, A. Trombettoni, M. Inguscio, M. Zaccanti, G. Roati, and N. P. Proukakis, Phys. Rev. Lett. **124**, 045301 (2020).

[37] L. Amico, G. Birkl, M. Boshier, and L.-C. Kwek, New. J. Phys. **19**, 020201 (2017).

[38] J. G. Lee, B. J. McIlvain, C. J. Lobb, and W. T. Hill, III, Sci. Rep. **3**, 1034 (2013).

[39] S. Eckel, J. G. Lee, F. Jendrzejewski, C. J. Lobb, G. K. Campbell, and W. T. Hill, III, Phys. Rev. A **93**, 063619 (2016).

[40] A. Burchianti, F. Scazza, A. Amico, G. Valtolina, J. A. Seman, C. Fort, M. Zaccanti, M. Inguscio, and G. Roati, Phys. Rev. Lett. **120**, 025302 (2018).

[41] J. M. Martinis, Les Houches **79**, 487 (2004).

[42] Y. M. Bidasyuk, M. Weyrauch, M. Momme, and O. O. Prikhodko, J. Phys. B: At. Mol. Opt. Phys. **51**, 205301 (2018).